

# Frequency Stability of Hybrid Power System in the Presence of Superconducting Magnetic Energy Storage and Uncertainties

M. Jalilian, A. Rastgou<sup>\*</sup>, S. Kharrati, S. Hosseini-Hemati

Department of Electrical Engineering, Kermanshah Branch, Islamic Azad University, Kermanshah, Iran

**Abstract**— Nowadays, in order to improve the dynamic performance of power networks and frequency control, LFC system is used in power plants. The presence of photovoltaic (PV) and wind turbine (WT) sources causes momentary changes in production and complicates the network frequency control process. In this paper, the random programming method with the Latin hypercube sampling pattern (LHS) is used to model the uncertainties of generating PV and PW sources. Also, to reduce the impact of the uncertainty of PV and PW sources on the frequency fluctuation, superconducting magnetic energy storage (SMES) has been used. Due to the fast dynamic response and favorable inertia characteristic of SMES, the performance of LFC and the stability of the system have been ameliorated. The simulation results in MATLAB software show that by step changes in the system load to the value of 0.1 pu, in the presence of SMES storage, the maximum overshoot value and the settling time of the system frequency are 16 percent and 3.2 seconds less, respectively.

**Keywords**— Dynamic performance, LFC, Power generation uncertainty, SMES, Solar-thermal power generators (STPG).

## NOMENCLATURE

DEG	Diesel engine generator
DG	Distributed generator
FOs	Frequency oscillations
LFC	Output current, the unit is (A)
LHS	Latin hypercube sampling
MG	Microgrid
PDF	Probability density function
PID	Proportional-integral-derivative
PV	Photovoltaic
SMES	Superconducting magnetic energy storage
STPG	Solar-thermal power generators
WTG	Wind turbine generator

## 1. INTRODUCTION

New technological developments in power systems, especially the attachment of renewable energy sources and the approach towards free trade in electricity markets, have expanded new opportunities and perspectives for electrical energy storage techniques. In addition, the significance and various applications of electrical energy storage technologies have doubled in the past decade due to advancements in corresponding scientific fields. These subjects have caused a fundamental need to evaluate and analyze the specific features of each technology and field. Large-scale energy storage technologies have played a significant role in energy management. These technologies' applications include peak smoothing, load curve leveling, energy arbitrage, and frequency stabilization usages [1].

Utilizing large capacity energy storage devices to balance the consumption curve and increase the load factor is one of the initial

applications of storing energy in power systems for economic purposes [2].

Furthermore, various grid disturbances contribute to some consequences such as sudden change load, disconnection of transmission lines, and system destabilization out of its equilibrium point. Under these circumstances, first, the energy is harvested from the kinetic energy of the synchronous generators' axis; next, the system control loops become activated and balance the system. This process generates oscillations of various parameters such as frequency and electrical power on the lines, which results in different challenges in the power system operation. In the case of storing an energy amount in the system, the mentioned challenges can be significantly reduced through a quick exchange of the stored energy with the grid in the requisite situations. In other words, the energy storage device can also be exploited to enhance the system's dynamic performance [3].

After the advent of superconductivity, various applications were presented for this physical phenomenon. One of its most well-known applications is superconducting magnetic energy storage (SMES) systems. In SMES, energy is stored in a coil with large inductance made of a superconductor. The coil's superconductivity feature leads to high back and forth efficiency of the energy storage process (about 95%). The high efficiency of SMES systems creates a significant advantage point compared to other energy storage techniques. In addition, SMES systems have a prompt dynamic response since electrical energy is converted to magnetic energy and in reverse in this technique. Thus, it is also applied to ameliorate dynamic performance [4].

In large-scale power systems, which usually consist of an interconnected control area, load frequency controls (LFC) is crucial for maintaining the system frequency and inter area tie power in the planned value range as much as possible. The input mechanical power to the generator is exploited to control the output electrical power frequency and maintain the scheduled power exchange between areas. In a deregulated power system, each control area includes different types of uncertainty and various disturbances due to increasing complexity, system modeling errors, and power system structure changes. An appropriately designed and operated power system must be strong to load changes and system disturbances. Moreover, it must also provide an acceptable

Received: 17 Nov. 2021

Revised: 07 Aug. 2022

Accepted: 20 Nov. 2022

\*Corresponding author:

E-mail: [abdollah.rastgo@gmail.com](mailto:abdollah.rastgo@gmail.com) (A. Rastgou)

DOI: 10.22098/joape.2023.9829.1686

**Research Paper**

©2023 University of Mohaghegh Ardabili. All rights reserved

level of electric power quality while maintaining voltage and frequency within tolerance limits [5].

Uncertain output power of renewable energy sources such as PV and WTG makes MG voltage and frequency control a challenging task that requires more effort and new adaptive control mechanisms. In [6], an adaptive control method has been developed to control the frequency and voltage of a microgrid using the reinforcement learning method. Reinforcement learning is one of the branches of machine learning, which is the main solution method of the Markov decision process. Among several methods for solving reinforcement learning, in this article, the Q learning method is used to solve reinforcement learning because it is a model-free strategy and has a simple structure. In [7], an innovative multi-stage controller for adjusting the load frequency of an independent microgrid has been presented. And to calculate the parameters of the controller, the Bonobo optimization algorithm is used.

In the new power systems such as microgrids (MGs) with low distributed generation (DG) sources and high inertia, only using the LFC method is not sufficient for load frequency stability and power balance. Energy storage sources are a valuable solution to improve transient stability and load frequency changes [8].

In [9], a new method based on power generation uncertainties and the use of energy storage features in microgrid frequency control is presented. The goals of this article include:

- management and control of energy storage unit, especially batteries, in order to create a frequency support mechanism in the microgrid.
- Managing and protecting the battery against changes in the charge and discharge current, reducing the transient fluctuations affecting the battery and also preventing the sudden interruption of the battery power.

Based on this, the frequency control method based on modeling uncertainties as well as the use of Lyapunov function stability equations and the optimal distribution of active power between power sources and storage units has been described.

Load demand response (DR) has emerged as a key component of power system frequency reliability and stability. In [10], the effect of DR regulation and hybrid energy storage (HES) on a two-zone experimental power system that includes photovoltaic sources, wind turbine, biogas unit and a thermal power plant has been investigated. By analyzing the system before and after DR, it has reached favorable conditions in terms of stability margin.

In [11] WT and Compressed Air Energy Storage (CAES) have been used to model frequency stability. Dynamic frequency maintenance using demand response (DR) program and injection of fast response CAES have been proposed in this paper. This problem is presented as a mixed integer nonlinear programming (MINLP) problem considering DR and WT uncertainties on a 6-bus test system. Among the various energy storage elements, SMES is a suitable choice because of its fast dynamic response and favorable inertial characteristic. Using accurate SMES modeling, the power stored during off-peak times can be used to inject the required power during sudden load changes to create stable frequency and power balance.

In addition, the uncertainty of PV sources and wind turbine WT, which are considered as disturbance input to MG, was compensated by using SMES [12, 13]. In [14], the frequency stability of the hybrid power system in the presence of superconducting storage (SMES) is discussed. In this paper, the transient stability of the system is enhanced in the presence of SMES and modified LFC. The modified LFC provides a more stable load frequency. Furthermore, the frequency fluctuation in the proposed control structure is reduced by an average of 15-20% compared to other methods.

In most of the mentioned articles, energy storage devices have been used in order to improve the stability of the transient state of the system in the conditions of uncertainty of PV and WT renewable energy sources. But the uncertainty modeling of PV

and WT resources is not mentioned. In this article, the random programming method with the Latin hypercube sampling pattern (LHS) is used to model the uncertainties caused by the production power of the solar source and wind turbine. Also, thermal-solar power plant is used as a new technology in the field of steam production instead of steam boiler and working cycle of turbine and dilator. Dynamic modeling of thermal-solar power plant is also presented as a new idea in this paper.

The primary aims of the present paper include the following:

- Modeling of thermal-solar power plant.
- The impact of uncertainty of PV and WT energy sources on grid frequency control.
- Using the stochastic programming method in order to model the uncertainty of PV and WT.
- The effect of SMES storage in improving frequency stability.

After the introduction, the second section of the present paper attends to modeling the under-examination systems, which are offered in two modes of islanded and grid-connected. In the third section, mathematical modeling of the investigated problem is presented. In this modeling, the SMES mathematical equation, WTG model, modeling of DEG, and STPG model are explained. In the fourth section, the stochastic optimization method and the LHS model are applied to model the uncertainties caused by the generated power of the solar power resource and WTG. The fifth section of the present study defines the simulation scenarios and evaluates their corresponding simulation results. Ultimately, in the sixth section, the conclusion of the study is presented.

## 2. INVESTIGATED HYBRID POWER SYSTEMS MODEL

In the present paper, two general modes have been considered for the studied hybrid power system.

- Islanded mode (off-Grid) of hybrid power system
- Grid-connected (on-Grid) hybrid power system

### 2.1. Islanded mode of hybrid power system

The islanded mode of the hybrid power system that is part of the study's simulation includes diesel engine generator (DEG), wind turbine generator (WTG), and solar-thermal power generators (STPG). In this section, three solution scenarios have been considered for the paper's validation. Scenario 1 indicates the simulation of islanded power system including DEG, WTG, and STPG; Scenario 2 represents the simulation of islanded power system including DEG and STPG; Scenario 3 is the simulation of islanded power system including DEG and WTG. In this regard, Fig. 1 demonstrates the block diagram of the islanded power system for three stated scenarios. SMES superconducting energy storage devices are utilized in all three scenarios. The power balance in all three scenarios is defined according to Equation 1 [15].

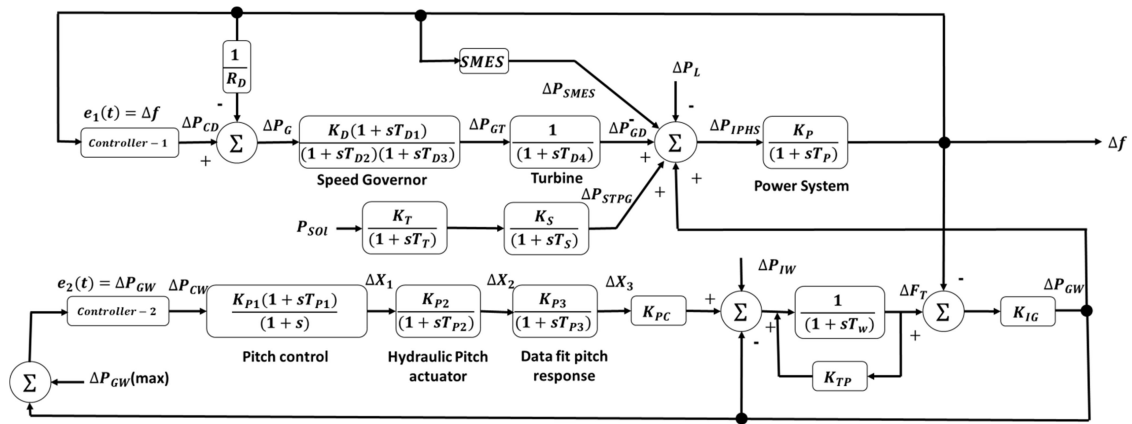
$$\Delta P_{IHPS} = \Delta P_{GD} + \Delta P_{STPG} + \Delta P_{GW} - \Delta P_L - \Delta P_{SMES} \quad (1)$$

In the above equation,  $\Delta P_{IHPS}$  represents the total IHPS power deviation,  $\Delta P_{GD}$  indicates the diesel engine generator output power deviation,  $\Delta P_{GW}$  is the wind turbine generator output power deviation,  $\Delta P_{STPG}$  specifies the STPG power deviation,  $\Delta P_{SMES}$  shows the SMES output power deviation, and  $\Delta P_L$  is the demand load change.

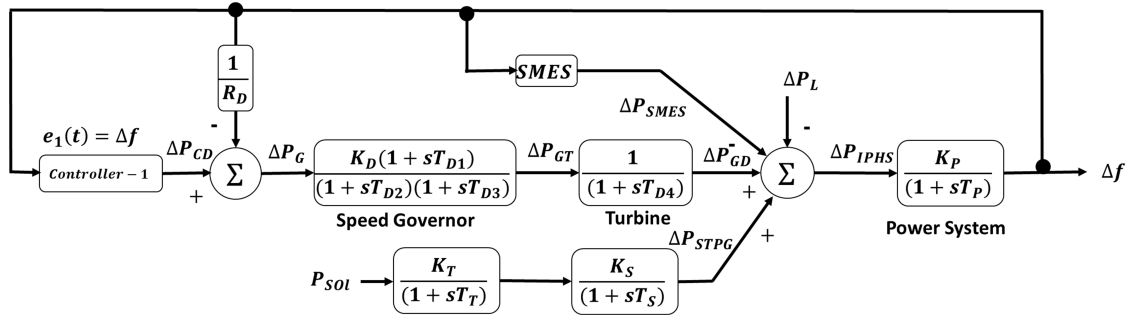
### 2.2. Grid-connected hybrid power system

The grid-connected hybrid power system consists of a wind turbine generator (WTG) and a solar-thermal power generator (STPG), as it is demonstrated in Fig. 2. The power balance in a grid-connected hybrid power system is presented in Equation 2 [15].

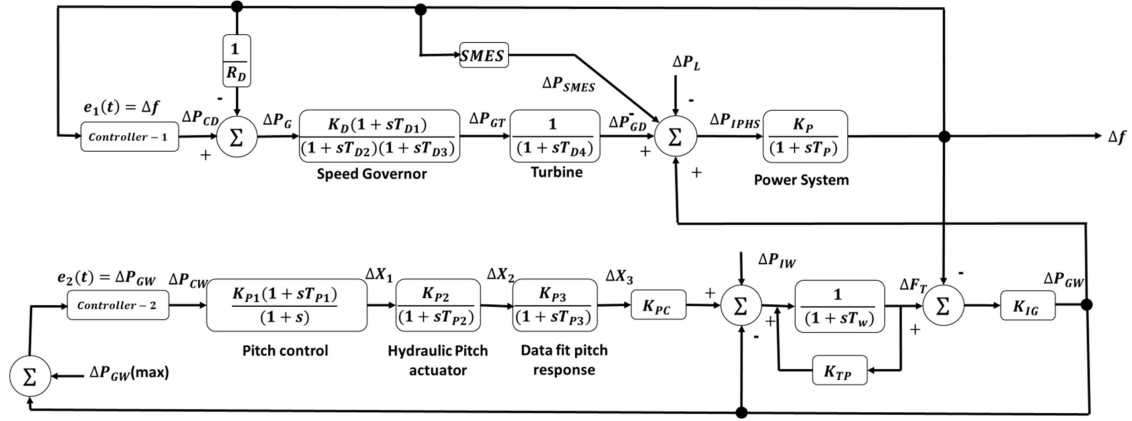
$$\Delta P_{GHPS} = \Delta P_{GW} - \Delta P_L + \Delta P_M \quad (2)$$



(a) Scenario 1



(b) Scenario 2



(c) Scenario 3

Fig. 1. Block diagram of the islanded power system for three different scenarios. (a) Scenario 1, (b) Scenario 2, and (c) Scenario 3 [15]

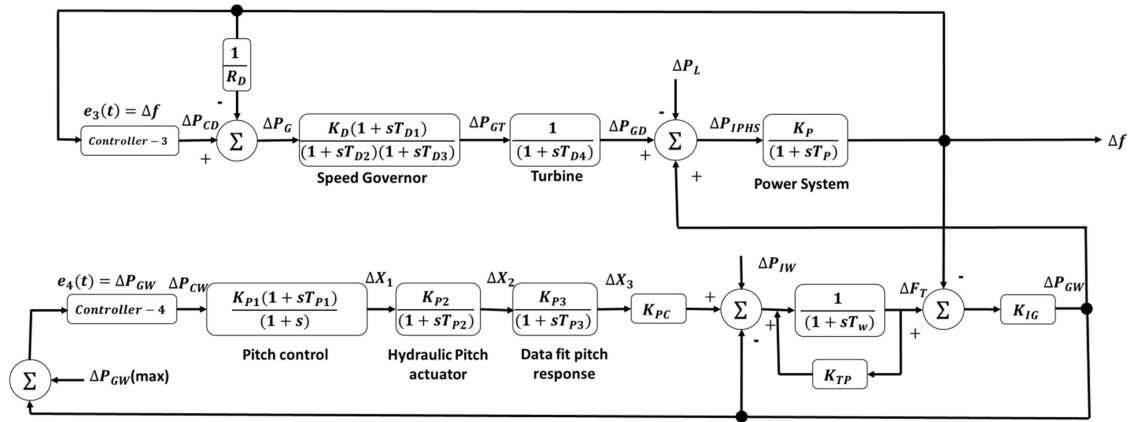


Fig. 2. Block diagram of the grid-connected hybrid power system.

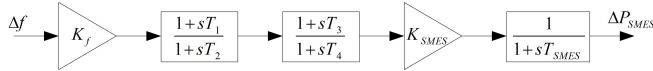


Fig. 3. block diagram of SMES [15]

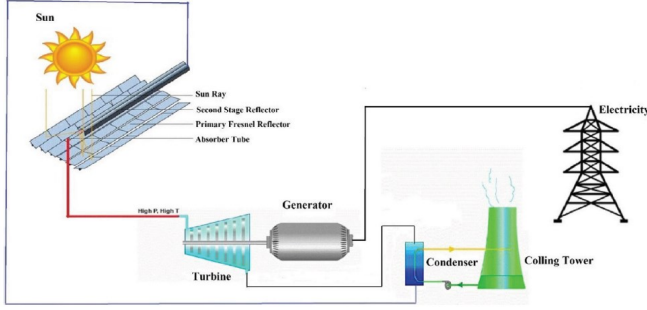


Fig. 4. The investigated solar thermal power plants [16]

In the presented equation,  $\Delta P_{GHPS}$  is the total GHPS power deviation  $\Delta P_{GW}$  is the wind turbine generator output power deviation,  $\Delta P_M$  is the steam turbine output power deviation.

### 3. MATHEMATICAL MODELING OF THE PROBLEM

#### 3.1. SMES Mathematical equation

The dynamic model of SMES in terms of changes in grid's frequency is presented in Fig. 3, and its transfer function is according to Equation 3. As it can be noted, the transfer function input is the frequency changes, and its output is the required SMES output power modifications to minimize the frequency fluctuations.  $T_{SMES}$ ,  $T_1$ ,  $T_2$ ,  $T_3$ , and  $T_4$  are the time constants of the SMES, and  $k_f$  and  $k_{SMES}$  are the gains of the SMES control system [15].

$$\Delta P_{SMES} = \left[ \frac{1}{1 + sT_{SMES}} \right] \left[ \frac{1 + sT_1}{1 + sT_2} \right] \left[ \frac{1 + sT_3}{1 + sT_4} \right] \Delta f \times K_f \times K_{SMES} \quad (3)$$

#### 3.2. Diesel engine generator model

Diesel engine generators play an important role in the islanded power system. The generated power of other power plants, such as wind turbines and solar-thermal power plants relies on ambient weather conditions. Therefore, they have lower reliability than diesel engine generators. In this study, a simplified model of governor, turbine, and combustion engine has been used. The transfer function of the diesel engine generator model is defined through Equations 4–6 [15].

$$\Delta P_{GD} = \left[ \frac{1}{1 + sT_{D4}} \right] \Delta P_{GT} \quad (4)$$

$$\Delta P_{GT} = \left[ \frac{K_D(1 + sT_{D1})}{(1 + sT_{D2})(1 + sT_{D3})} \right] \Delta P_G \quad (5)$$

$$\Delta P_G = \Delta P_{CD} - \left( \frac{1}{R_D} \right) \Delta f \quad (6)$$

In the stated equations,  $\Delta P_G$  represents the control signal of governor speed in terms of per unit,  $\Delta P_{GT}$  indicates the diesel engine generator control signal in terms of per unit,  $\Delta P_{CD}$  specifies the control signal for diesel engine governor,  $\Delta f$  is the frequency deviation,  $R_D$  shows the regulator of governor's speed,  $K_D$  indicates the governor gain;  $T_{D1}$ ,  $T_{D2}$ , and  $T_{D3}$  are the time constants of the governor speed (per second) and  $T_{D4}$  is the time constant of the turbine.

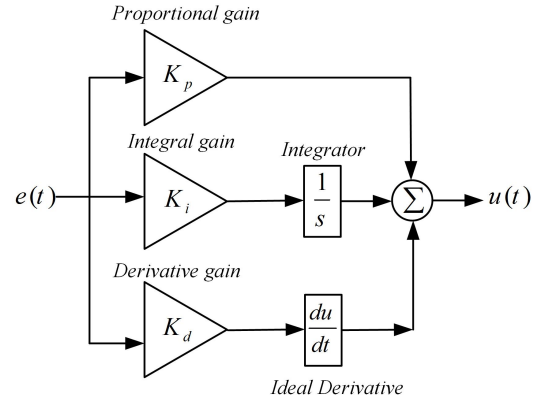


Fig. 5. PID controller [8]

#### 3.3. Wind turbine model

A wind farm converts the resulted mechanical energy of wind into electrical energy. The aerodynamic power of a wind turbine is presented in Equation 7 [15].

$$p_t = \frac{1}{2} C_p(\eta, \beta) \rho \pi R^2 v^3 \quad (7)$$

In the mentioned equation,  $\rho$  is the air density,  $R$  represents the blade radius,  $\beta$  indicates the steep angle,  $v$  specifies the linear speed of the wind, and  $C_p$  is the power factor. Moreover, the transfer function equation of the wind farm is demonstrated in Equation 8. The fluid coupling block is dedicated to model the frequency difference of wind turbine and generator, which is shown in Equation 8.

$$\Delta P_{GW} = K_{IG}[\Delta F_T - \Delta f] \quad (8)$$

In the above equation  $K_{IG}$  is the fluid coupling gain and  $\Delta F_T$  is the wind turbine generator speed deviation.

#### 3.4. Solar-Thermal power plant

Solar-Thermal power plants are similar to thermal power plants, except that the required generated steam for rotating the turbine that is supplied by solar energy. It has a similar closed cycle of thermal power plants, in which the steam transforms into the water after passing through the condenser and is retransformed to steam through the solar cell's energy. In this regard, Fig. 4 demonstrates an instance of solar thermal power plants [16].

The solar-thermal power plant is exploited as a novel technology instead of using a boiler, turbine cycle, and dilator in the steam generation field. Thus, it is a typical solar thermal power plant with a different steam generation process. The transfer function of a solar thermal power plant is presented in Equation 9 [15].

$$G_{STPG}(s) = \left[ \frac{K_T}{1 + sT_T} \right] \left[ \frac{K_S}{1 + sT_S} \right] = \frac{\Delta P_{STPG}}{\Delta P_{SOL}} \quad (9)$$

In the mentioned equation  $K_T$  and  $K_S$  are the STPG gains,  $T_T$  and  $T_S$  are the STPG time constants. Moreover,  $\Delta P_{STPG}$  and  $\Delta P_{SOL}$  are the input and output power differences of STPG.

#### 3.5. PID controller

In the hybrid power system stabilizer, some controllers are responsible for frequency stability. These controllers usually utilize a PID controller to eliminate the difference between the frequency reference value and the measured value. The PID controller is the most well-known and widely applied feedback mechanism. Due to its highly convenient structure and impressive function, it is exploited in a wide range of industrial processes. In Fig. 5, the PID controller structure has been demonstrated.

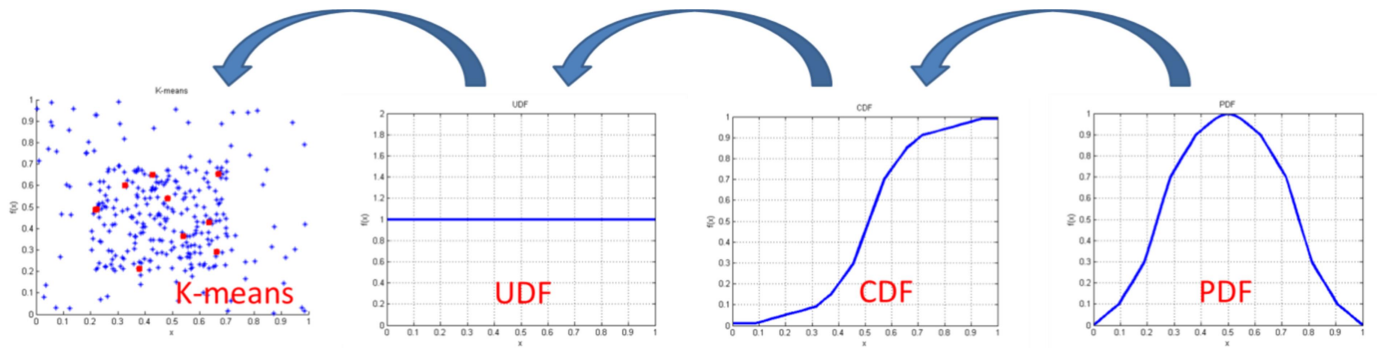


Fig. 6. Procedures of LHS sampling and K-means clustering methods

### 3.6. Wind and solar generator uncertainty

Wind flow speeds are continuously modifying, and a precise and particular speed cannot be determined for a specific geographical region. To determine the frequency of wind speed in a particular area, an appropriate probability function can be obtained for determining wind changes by referring to the previously recorded wind speeds in that area. In this paper, the Weibull distribution function is utilized to model wind changes [17].

$$f_w^t(v) = \left(\frac{k^t}{c^t}\right) \left(\frac{v^t}{c^t}\right)^{k^t-1} \exp\left(-\left(\frac{v^t}{c^t}\right)^{k^t}\right) \quad \text{for } c^t > 1, k^t > 0 \quad (10)$$

Shape and scale parameters of Weibull distribution are significant for each period. For these parameters, the following equation governs:

$$k^t = \left(\frac{\sigma_v^t}{\mu_v^t}\right)^{-1.086} \quad (11)$$

$$c^t = \frac{\mu_v^t}{T(1 + \frac{1}{k^t})} \quad (12)$$

The mean and standard deviation of wind speed are determined based on historical data for each period.

The turbine characteristics, particularly cut-in and cut-out speeds of the turbine, are required to calculate the wind turbine output power according to wind speed at time t. Furthermore, Equation 13 is presented in the following.

$$P_{wt}^t = \begin{cases} P_{wt,r} & v_r < v^t < v_{cout} \\ P_{wt,r} \frac{v^t - v_{cin}}{v_r - v_{cin}} & v_{cin} < v^t < v_r \\ 0 & \text{otherwise} \end{cases} \quad (13)$$

The output power of the photovoltaic (PV) solar panel depends on the incident solar radiation, the absorption capacity, the panel surface area, and the cell temperature. The incident solar radiation is a probabilistic parameter; thus, the corresponding output power is alternating. In many studies such as [18, 19], the probability density function (PDF) of beta distribution has been applied to describe the PV behavior, which is defined as follows

$$f_{pv}^t(s_i^t) = \begin{cases} \frac{T(\alpha^t + \beta^t)}{T(\alpha^t)T(\beta^t)} (s_i^t)^{\alpha^t-1} (1 - s_i^t)^{\beta^t-1} & \text{for } \alpha^t > 0, \beta^t > 0 \\ 0, & \text{otherwise} \end{cases} \quad (14)$$

The parameters of the beta distribution function depend on the standard deviation and the radiation data and are determined for each period as follows:

$$\beta^t = (1 - \mu_s^t) \left( \frac{\mu_s^t(1 - \mu_s^t)}{(\sigma_s^t)^2} - 1 \right) \quad (15)$$

$$\alpha^t = \frac{\mu_s^t \beta^t}{1 - \mu_s^t} \quad (16)$$

The output power of solar panels is calculated based on the incident solar radiation on their surface for different levels of absorption capacity in the examined period based on the following equation:

$$P_{pv}^t = \eta_{pv} r^t S_{pv} \quad (17)$$

## 4. STOCHASTIC PROGRAMMING METHOD

Stochastic programming is a mathematical optimization model in which all input parameters are not deterministic, and non-deterministic parameters are settled by probabilistic distributions. Stochastic programming is exploited in many fields, including wind and solar renewable power generation fields.

### 4.1. Scenario generation and clustering

Latin hypercube sampling (LHS) method has been used to analyze the uncertainties caused by the generated power of photovoltaic panels and wind turbines. This technique is divided into two stages of sampling and pairing (Fig. 6). In the sampling stage, the following steps are applied to each random variable (wind speed and solar radiation).

- 1) The cumulative distribution function of wind speed and solar radiation is divided into 500 intervals with a probability of 1/500.
- 2) A random uniform number is selected for each interval using a uniform distribution such that:  $U_i \in (0, 1)$ .
- 3) The cumulative probability of the sample generated in step 2 for each interval is equal to:

$$Prob_i = \left(\frac{1}{1000}\right) U_i + \left(\frac{i-1}{1000}\right) \quad (18)$$

- 4) Using the inverse of the cumulative distribution function, the value of  $x_i$  random variable is calculated based on the cumulative probability of the  $Prob_i$  sample.

$$x_i = F^{-1}(Prob_i) \quad (19)$$

- 5) Steps 2 to 4 are iterated 500 times for each random variable. In stochastic programming, the simulation's computational load and execution time is increased by increasing the number of scenarios. To resolve this issue, the K-means clustering algorithm is applied to reduce the number of scenarios. The K-means clustering method carries out the clustering process according to the smallest distances of each data from the centers of a cluster (average) to encompass the data in K clusters. This process is performed such that the sum of the squares of data distances from the cluster center is minimized, in other words:

$$J = \sum_{j=1}^k \sum_{i=1}^n \|x_i^{(j)} - c_j\|^2 \quad (20)$$

Where  $\| \cdot \|$  indicates the normed distance between the points of  $x_i^{(j)}$  and  $c_j$ , the center of the j cluster.

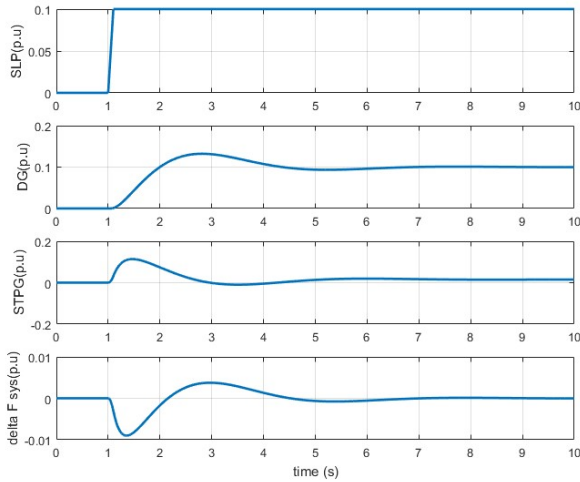


Fig. 7. Damping process of frequency oscillations of the studied system in Scenario 1

## 5. DEFINING SIMULATION SCENARIOS

To evaluate the frequency stability of the under investigation system (Fig. 1(a)) and to examine the impacts of each of the power generation sources and SMES devices, three scenarios are defined in the following. Each of these will be separately investigated and analyzed.

- Power system frequency stability in the presence of diesel engine generator power source, equipped with the governor, and solar-thermal power plant
- Power system frequency stability in the presence of diesel engine generator power source equipped with the governor, solar-thermal power plant, and SMES
- Power system frequency stability with the presence of diesel engine generator power source equipped with the governor, solar-thermal power plant, SMES, and wind farm
- Investigating the impression of solar and wind resources power generation uncertainty in grid frequency control

To simulate the defined scenarios, the information of each power generation unit, energy storage devices, and the under investigation grid is required. According to reference [16], the required information is presented based on the following tables. Table 1 demonstrates the dynamic parameters of the wind farm, diesel engine generator, solar-thermal power plant, and SMES device. The characteristics of the utilized rotor in the wind farm are displayed in Table 2. Moreover, the characteristics of the diesel engine generator shaft are exhibited in Table 3.

### 5.1. Scenario 1: Power system frequency stability in the presence of diesel engine generator power source, equipped with the governor, and solar-thermal power plant

In this scenario, two power resources, including diesel generator (DG) and solar-thermal power generator (STPG), are considered as the base power plants of study. By applying 0.1 per unit frequency (SLP) changes to the electrical grid, the compensation procedure of the PID control system of the diesel generator governor is studied. As shown in Fig. 1(a), the electrical grid's output is the frequency changes that occurred due to changes in the step load and is sent to the PID controller input for comparison as the error signal. In the PID controller system, the zero reference value is assumed as the absence of frequency changes, and through comparing the frequency changes amount, an error is created for the PID controller system. In this regard, the PID controller causes the generation of a stabilizing signal at the diesel generator output by applying a control signal to the diesel generator governor.

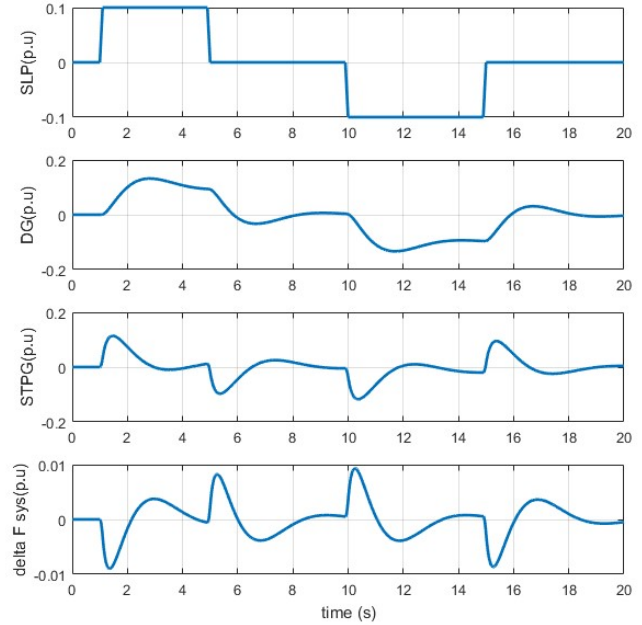


Fig. 8. Damping process of frequency oscillations of the studied system in Scenario 1 for variable load

Furthermore, it dampens the oscillation by compensating for the extra power load. Fig. 7 displays the damping process of frequency oscillations of the studied system in Scenario 1 for a step load. As can be observed, in 1 second, the grid frequency changes 0.1 per unit stepwise that causes a frequency drop in the output of the electrical grid. At this moment, the PID controller of the diesel generator governor operates and dampens the grid frequency by generating a stabilizing signal. In other words, the added load is compensated by the power generator units.

As it is shown in Fig. 7, increasing the power system load by 0.1 p.u. causes the frequency to drop. In this scenario, the amount of frequency drop is 0.0098, with 0.13p.u DG active power compensation and 0.11p.u STPG active power compensation, they have succeeded in damping the frequency fluctuations in the settling time of 5 seconds.

In this regard, Table 4 represents the frequency oscillation indices of the studied grid in Scenario 1. As presented, a high overshoot (90%) in a prompt rise time occurs after load changes. On the other hand, the 7.2 second settling time for damping oscillations is long and stressful, which drives the system toward its instability limit.

Frequency oscillations can be originated from sudden changes in load in an increasing or decreasing manner. The variable load is utilized for the studied system to investigate oscillations in both cases. Fig. 8 presents the damping process of frequency oscillations of the studied system in Scenario 1 for the variable load.

As shown in Fig. 8, the network load increased by 1 step at 1 and 15 seconds and decreased by 1 step at 5 and 10 seconds. And it has caused a reduction in frequency at the moment of load increase and a growth in frequency at the moment of load decline. The PID controller of the diesel generator governor system has performed optimally in two states of decreasing and increasing the frequency and has led to optimal DG control.

As can be noted, the PID controller represents a favorable performance in two states of increasing and decreasing the system load and grid frequency oscillations. Moreover, it has caused the optimal control of the diesel generator governor system.

Table 1. Dynamic parameters of the wind farm, diesel engine generator, solar-thermal power plant, and SMES device

Model	Parameters				
Wind unit	$K_{P1} = 1.25, K_{PC} = 0.08$	$K_{P2} = 1.25, T_{P1} = 0.60 \text{ sec}$	$K_{P3} = 1.40, T_{P2} = 0.041 \text{ sec}$	$K_{TP} = 0.0033, T_{P3} = 1.0 \text{ sec}$	$K_{IG} = 0.9969$
Diesel unit	$K_D = 0.3333, T_{D4} = 3.0 \text{ sec}$	$R_D = 3.0 \text{ Hz/p.u}$	$T_{D1} = 1.00 \text{ sec}$	$T_{D2} = 2.00 \text{ sec}$	$T_{D3} = 0.025 \text{ sec}$
Thermal unit	$T_g = 0.8 \text{ sec}$	$T_t = 0.3 \text{ sec}$	$R_D = 2.4 \text{ Hz/p.u}$	$k_P = 120$	$T_P = 14.4 \text{ sec}$
SMES	$K_F = 0.3333$				
Solar unit	$K_S = 1.8$	$K_T = 1$	$T_S = 1.8 \text{ sec}$	$T_T = 0.3 \text{ sec}$	

Table 2. The characteristics of the utilized rotor in the wind farm

Rotor characteristic	Value
Minimal rotor speed	9 rpm
Rated rotor speed	8 rpm
Rotor diameter	60 m
Rotor swept area	2827 m <sup>2</sup>
Rated wind speed	14 m/s
Inertia constant	0.72 s

Table 3. The characteristics of diesel engine generator shaft

Shaft characteristic	Value	Variable
Rated power	1.5 MW	$P_{shaft}$
Rated speed	18 rpm	$\omega_n$
Turbine damping	$14 \times 10^6 \text{ Nms/rad}$	$D_{turb}$
Rotor inertia	$6.1 \times 10^6 \text{ Kg/mm}$	$J_{turb}$
Shaft stiffnes	$83 \times 10^6 \text{ Nm/rad}$	$K_s$

**5.2. Scenario 2: Power system frequency stability in the presence of diesel engine generator power source, equipped with the governor, solar-thermal power plant, and SMES**

In this scenario, similar to Scenario 1, the two power generation resources of the diesel generator and the solar-thermal power plant are considered as the base power plants; additionally, the SMES device is exploited for compensating purposes. In this system(Fig. 1(b)), the output grid’s frequency oscillations are applied to the input of the PID controller system and the SMES device’.

The electrical grid output is applied to the PID controller and the SMES device as an error signal. This oscillation caused by the injected energy of SMES into the grid compensates for the frequency change. Thus, it results in improving the system response and reduction of frequency oscillations. As demonstrated in Fig. 9, the SMES device initiates the power compensation as the step load increases and the frequency drops sharply; however, it cannot compensate for the overshoot due to its low compensatory capacity. Nevertheless, it assists the reduction of grid settling time.

It can be seen in Fig. 9, with a step increase in load and a sharp drop in frequency, the superconducting storage begins to compensate for the power. Since SMES has a fast dynamic response, it makes amends for active power and improves frequency fluctuations. However, due to the high system load changes and the limited capacity of SMES, active power compensation has also been done by DG and STGP.

Table 5 represents the frequency oscillations indices of the studied grid of Scenario 2. As can be seen, a high overshoot (82%) with a rapid rise time occurred after the load change. On the other hand, a 4.1 second settling time to dampen the oscillations is a more favorable value than the corresponding value of Scenario 1. Fi. 10 displays the Damping process of frequency oscillations of the studied system in Scenario 2 for the variable load. As can be observed, the SMES device initiates the power shortage compensation as the system load increases. However, it

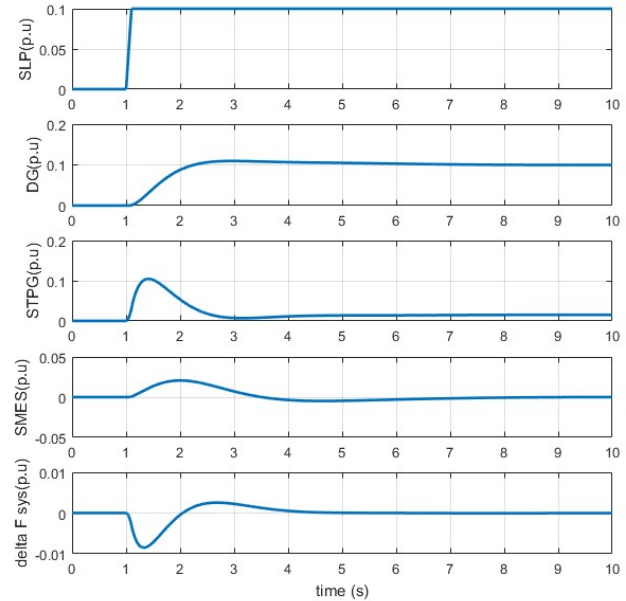


Fig. 9. Damping process of frequency oscillations of the studied system in Scenario 2

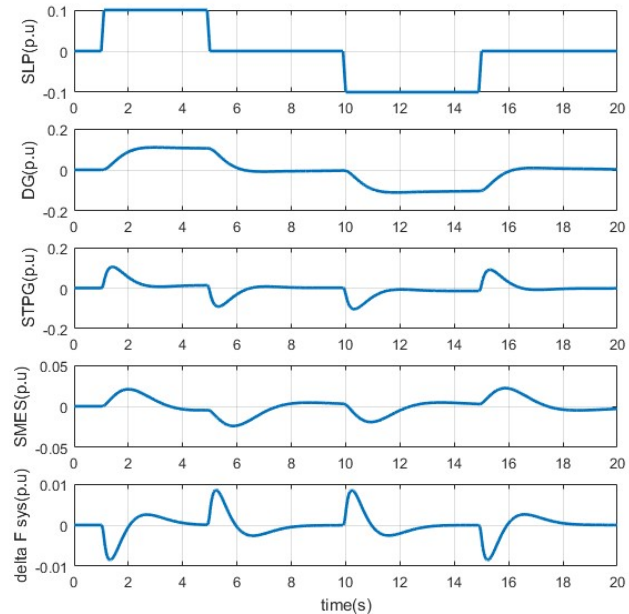


Fig. 10. Damping process of frequency oscillations of the studied system in Scenario 2 for variable load

Table 4. The frequency oscillation indices of studied grid in the Scenario 1

indicator	Overshoot (MP (%))	Rising time (tr (s))	Setting time (ts (s))
values	90	1.3	7.1

Table 5. The frequency oscillation indices of the studied grid in Scenario 2

indicator	Overshoot (MP (%))	Rising time (tr (s))	Setting time (ts (s))
value	82	1.3	4.1

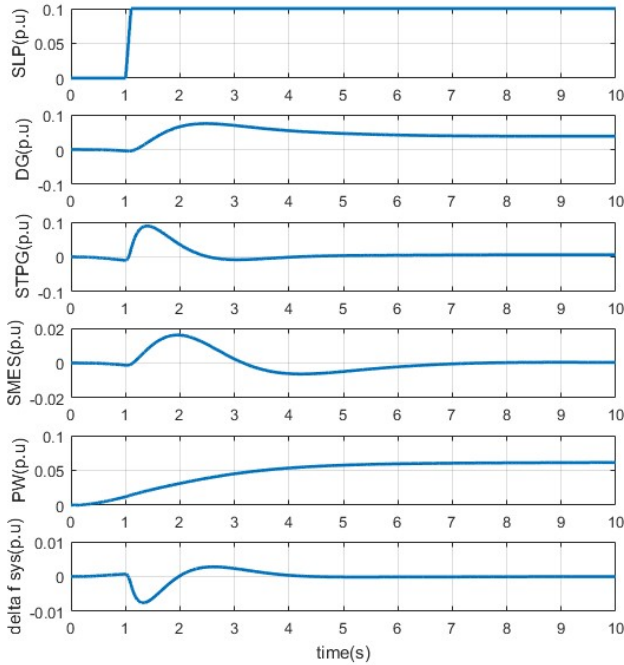


Fig. 11. Damping process of frequency oscillations of the studied system in Scenario 3

Table 6. The frequency oscillation indices of the studied grid in Scenario 3

indicator	Overshoot (MP (%))	Rising time (s)	Setting time (s)
values	75	1.3	3.9

begins to store energy and maintain frequency (damping frequency oscillations) when the load decreases.

In this scenario, SMES works in two discharge cycles in a time interval of 1 to 5 seconds and a charge cycle in a time interval of 10 to 15 seconds. in order to improve the frequency response of the system in sudden load changes.

**5.3. Scenario 3: Power system frequency stability in the presence of diesel engine generator power source, equipped with the governor, solar-thermal power plant, SMES, and wind farm**

Identical to Scenario 2(Fig. 1(c)), diesel generator and solar-thermal power plant are available as base power plants in this scenario. The SMES device acts as a power compensator in the studied grid; additionally, the wind farm is added to the system to provide power and further eliminate frequency oscillations. In this system, the frequency oscillations of the grid output are applied to the input of the diesel generator governor’s PID controller system, the input of the SMES device, and the input of the PID controller of the wind farm rotor. It is demonstrated in Fig. 11, as the step load increases and the frequency drops sharply, the two PID control systems in the diesel generator and the wind farm initiate the compensation of oscillations by increasing the governor power and the wind turbine rotor torque. Meanwhile,

Table 7. Response of three scenarios to step load changes

indicator	Overshoot (MP (%))	Rising time (s)	Setting time (s)
Scenario1	90	1.3	7.1
Scenario2	82	1.3	4.1
Scenario3	75	1.3	3.9

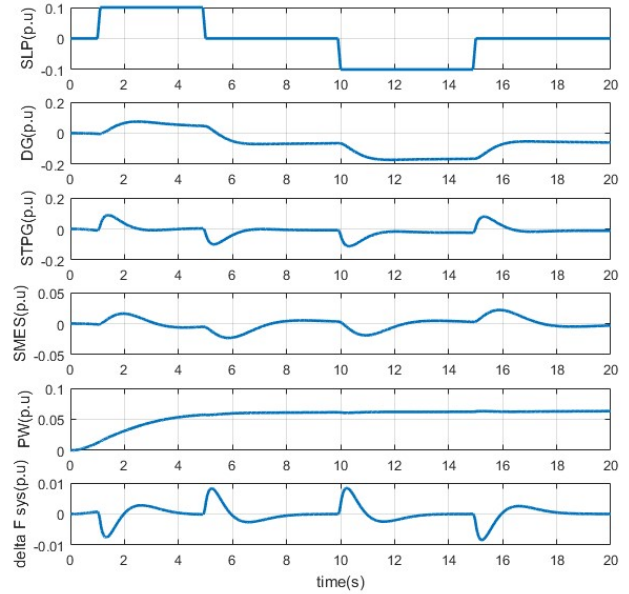


Fig. 12. Damping process of frequency oscillations of the studied system in Scenario 3 for variable load

the SMES device compensation begins. Through examining Fig. 11, it can be observed that the wind turbine compensation process is considerably slower than diesel generator, STPG, and SMES compensations. Nevertheless, the frequency compensation amount is significantly higher than the two mentioned units and storage device. Overall, it reduces the settling time of frequency oscillations and its overshoot. In this regard, Table 6 demonstrates the frequency oscillation indices of the studied grid in Scenario 3. As can be seen, a significantly high overshoot (75%) with a rapid rise time occurs after the load change. Nevertheless, a 3.9 second settling time to dampen the oscillations is more favorable than the corresponding value in Scenario 2.

Fig. 12 represents the damping process of frequency oscillations of the studied system in Scenario 3 for the variable load. As it can be perceived, the presence of wind farm improves the system oscillations response in two states of load increase and decrease.

In this scenario, in addition to the PID control system of the diesel generator governor, the PID control system of the wind turbine rotor also has the task of compensating the power in sudden changes in the system load. Also SMES operates in two cycles of charging (reducing load) and discharging (increasing load). in order to improve the frequency response of the system in sudden load changes.

**5.4. Comparison of the three scenarios results**

In the present paper, three scenarios of power system frequency stability in the presence of diesel generator power source equipped with the governor, solar-thermal power plant, SMES, and wind farm have been considered with the uncertainty of renewable resources power generation. The performance of each scenario was investigated with the grid’s step load changes. Table 7 presents the responses of the three scenarios to the step load changes.

**5.5. Impact of wind and solar resources uncertainty**

In this scenario, similar to Scenario 3, the dynamic stability of the grid frequency in the presence of SMES devices and PV and WT sources has been considered. However, in this scenario, the uncertainty of PV and WT sources power generation is also regarded in modeling.

Table 8. The most probable studied scenarios for solar radiation

$\omega$	$\pi(\omega)$	Value									
1	0.046	330.1	6	0.055	373.3	11	0.047	363.5	16	0.041	370.1
2	0.043	324.1	7	0.055	299.0	12	0.051	366.9	17	0.040	295.7
3	0.052	336.0	8	0.069	324.5	13	0.059	350.6	18	0.042	293.1
4	0.055	305.2	9	0.050	295.7	14	0.060	377.5	19	0.049	309.5
5	0.064	331.3	10	0.047	365.0	15	0.051	344.8	20	0.045	343.0

Table 9. The most probable studied scenarios for wind speed

$\omega$	$\pi(\omega)$	Value									
1	0.046	1.23	6	0.055	1.09	11	0.047	1.00	16	0.041	1.17
2	0.043	1.25	7	0.055	1.17	12	0.051	1.09	17	0.040	1.16
3	0.052	1.06	8	0.050	1.02	13	0.059	1.27	18	0.042	1.24
4	0.055	1.24	9	0.050	0.99	14	0.068	1.14	19	0.049	1.03
5	0.064	1.00	10	0.047	1.00	15	0.051	1.05	20	0.045	0.99

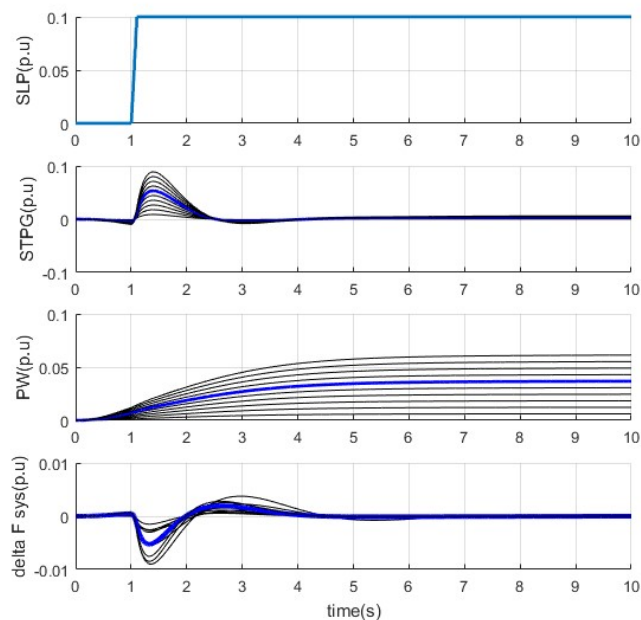


Fig. 13. Damping process of frequency oscillations of the studied system in Scenario 4

In the present scenario, the problem is modeled through stochastic programming. To solve the problem, examinations are carried out in one peak hour of PV and WT resources. In these investigations, 20 scenarios (out of 500 scenarios), each of which encompasses the generation of PV unit, WT source, are generated and utilized using K-means clustering algorithm. Table 8 exhibits the most probable studied scenarios for solar radiation and wind speed.

To investigate the impression of damping PV and WT sources in their generation's uncertainty conditions, 20 occurred scenarios for solar radiation and wind speed are considered, and the problem simulation is iterated for step load changes. Fig. 13 demonstrates the damping process of frequency oscillations of the studied system in Scenario 4 for step load changes. As it can be observed, the PV and WT units' uncertainties have been presented for 20 system oscillation responses in load step changes conditions. It has been achieved by examining the investigated scenario that the studied system is robust to PV and WT power generation uncertainties. Furthermore, it has the ability to damp oscillations in uncertainty conditions.

## 6. CONCLUSION

In this article, energy storage systems based on superconductivity (SMES) were used to improve load frequency oscillations in the hybrid power system including diesel generator power generation source, PV renewable energy and solar thermal power plant. Also a control strategy for frequency control such as PID controller was proposed. In the article, the uncertainty modeling of PV and PW production resources is based on stochastic planning, mostly using the Latin hypercube Sampling (LHS) method. The simulation for two step loads and variable loads based on four scenarios was performed separately in the MATLAB software. The simulation results show that with step changes in the system load to the value of 0.1 pu, in the presence of SMES storage, the maximum overshoot value and the settling time of the system frequency are 16% and 3.2 seconds less, respectively.

## REFERENCES

- [1] R. Ali, T.H. Mohamed, Y.S. Qudaih, Y. Mitani, "A new load frequency control approach in an isolated small power systems using coefficient diagram method," *Electr. Power Energy Syst.*, vol. 56, pp. 110–116, 2014.
- [2] H. Holttinen, R. Hirvonen, "Power system requirements for wind power", in: T. Ackermann (Ed.), *Wind Power in Power Systems*, John Wiley & Sons Ltd, Chapter 8, 2005.
- [3] M. Gouveia Eduardo, A. Matos Manuel, "Evaluating operational risk in a power system with a large amount of wind power," *Electr. Power Syst. Res.*, vol. 79, pp. 734–739, 2009.
- [4] Senju Tomonobu, et al., "A hybrid power system using alternative energy facilities in isolated island," *IEEE Trans Energy Convers.*, vol. 20, no. 2, pp. 406–414, 2005.
- [5] D. Rekioua, S. Bensmail, N. Bettar, Development of hybrid photovoltaic-fuel cell system for stand-alone application, *Int. J. Hydrogen Energy*, vol. 39, no. 3, pp. 1604–1611, 2014.
- [6] Shayeghi, H., and A. Younesi. "Mini/micro-grid adaptive voltage and frequency stability enhancement," *J. Oper. Autom. Power Eng.*, vol. 7, no. 1, pp. 107–118, 2019.
- [7] Shayeghi, H., and A. Rahnama. "Frequency Regulation of a Standalone Interconnected AC Microgrid Using Innovative Multistage TDF(1+ FOPI) Controller," *J. Oper. Autom. Power Eng.*, 2022.
- [8] Z.A. Obaid, L.M. Cipcigan, L. Abraham, "Frequency control of future power systems: reviewing and evaluating challenges and new control methods," *J. Mod. Power Syst. Clean Energy*, vol. 7, pp. 9–25, 2019.
- [9] R. Sephezrad, S. Nakhaeisharif, A. Al-Durra, M. Allahbakhshi, A. Moridi, "Islanded micro-grid frequency control based on the optimal-intelligent lyapunov

- algorithm considering power dynamic and communication uncertainties,” *Electr. Power Syst. Research*, Vol. 208, 2022.
- [10] A. Saxena, R. Shankar, “Improved load frequency control considering dynamic demand regulated power system integrating renewable sources and hybrid energy storage system,” *Sust. Energy Techno. Asses.*, Vol. 52, Part C, 2022.
- [11] M. Sedighizadeh, M. Esmaili, S.M. Mousavi-Taghiabadi, “Optimal joint energy and, reserve scheduling considering frequency dynamics, compressed air energy storage, and wind turbines in an electrical power system,” *J. Energy Storage*, vol. 23, pp. 220–233, 2023.
- [12] S. Takayama, R. Matsuhashi, “Development of model for load frequency control in, power system with large-scale integration of renewable energy,” *IEEE Power and Energy Conf. (PECI)*, Urbana, IL, pp. 1–8, 2016.
- [13] G. Magdy, G. Shabib, A.A. Elbaset, and Y. Mitani, “Optimized coordinated control of LFC and SMES to enhance frequency stability of a real multi-source power system considering high renewable energy penetration,” *Prot. Control Mod. Power Syst.*, vol. 3, no. 1, pp. 1–15, 2018.
- [14] Sahbasadat Rajamand, “Load frequency control and dynamic response improvement using energy storage and modeling of uncertainty in renewable distributed generators,” *J. Energy Storage*, Vol. 37, 2021.
- [15] Somnath Ganguly, Chandan Kumar Shiva, V. Mukherjee “Frequency stabilization of isolated and grid connected hybrid power system models,” *J. Energy Storage*, vol. 19, pp. 145–159, 2018.
- [16] Deepak Bishoyi, K. Sudhakar, Modeling and performance simulation of 100 MW LFR based solar thermal power plant in Udaipur India,” *Resource-Efficient Techno.*, vol. 3 opp. 365–377, 2017.
- [17] Ho WS, Macchietto S, Lim JS, Hashim H, Muis ZA, Liu WH. “Optimal scheduling of energy storage for renewable energy distributed energy generation system.” *Renew. Sustain. Energy Rev.* vol. 58, pp. 1100–7, 2016.
- [18] L.M. Ramirez-Elizondo , G.C. Paap, "Scheduling and control framework for distribution-level systems containing multiple energy carrier systems," *Electr. Power Energy Syst*, vol. 66, pp. 194–215, 2015.
- [19] Pazouki S, Haghifam M-R. Optimal planning and scheduling of energy hub in presence of wind, storage and demand response under uncertainty. *Int. J. Electr. Power Energy Syst.*, vol. 80, pp. 219–39, 2016.